

MEASUREMENT OF VISIBLE AND NEAR-IR OPTICAL PROPERTIES OF SOOT PRODUCED FROM LAMINAR FLAMES

JINYU ZHU,¹ MUN YOUNG CHOI,² GEORGE W. MULHOLLAND,³ SAMUEL L. MANZELLO,³
LOUIS A. GRITZO⁴ AND JILL SUO-ANTTILA⁴

¹*Department of Mechanical Engineering
University of Illinois at Chicago
Chicago, IL 60607, USA*

²*Department of Mechanical Engineering and Mechanics
Drexel University
Philadelphia, PA 19014, USA*

³*Building and Fire Research Laboratory
National Institute of Standards and Technology
Gaithersburg, MD 20899, USA*

⁴*Fire Science and Technology
Sandia National Laboratory
Albuquerque, NM 87185, USA*

This study describes the measurements of the dimensionless extinction constant, K_e , of soot in the visible and IR spectrum using the National Institute of Standards and Technology Large Agglomerate Optics Facility. Soot was produced using a 11 mm i.d. laminar diffusion flame burner fueled with acetylene and ethene. Light extinction measurements were performed using light sources at 543.5, 632.8, 856, 1314, and 1565 nm. The mean values of present measurements of K_e range from 7.95 to 10.0. These unique experiments provide accurate values of K_e to be used for measurements of soot concentration and temperature in the IR spectrum.

These measurements represent the first fuel-specific data available in the near-IR spectrum. The measured K_e values for all wavelengths are significantly larger than values calculated using reported values of the refractive index and the Rayleigh theory. Transmission electron microscopy and optical microscopy analyses were used to analyze soot morphology and aerosol properties to estimate the influences of beam shielding and light scattering on the observed variations of K_e .

Introduction

Particulate emission from mobile and stationary sources burning hydrocarbon fuels creates environmental and health hazards. It was recently estimated that 60,000 people die prematurely each year from soot inhalation [1]. Soot production is also one of the major causes of process inefficiency in energy conversion systems and causes deleterious fouling of hardware. Soot particles affect the environment in many ways, including contributions to the formation of photochemical smog [2,3] and atmospheric acids [4]. Soot particles released into the atmosphere scatter and absorb solar radiation that can degrade atmospheric visibility. Accurate measurement of soot emitted from these sources is therefore important for gauging the posed environmental hazards, health impacts, and fire safety issues.

Soot particle concentrations are typically measured using a non-intrusive light extinction technique. In this technique, the ratio of the transmitted to the incident light intensity is used to obtain the soot volume fraction, f_v ,

$$\frac{I}{I_0} = \exp\left(-K_e \frac{f_v}{\lambda} L\right) \quad (1)$$

where K_e is the dimensionless soot extinction constant, L is the path length through the soot, and λ is the wavelength of the light source. K_e computed in the Rayleigh-Debye limit is composed of the dimensionless absorption constant, K_a , and the dimensionless scattering constant, K_s [5],

$$K_a = 6\pi E(m); K_s = \frac{4\pi x_p^3 \overline{n^2} F(m)}{n^1} \left(1 + \frac{16\pi^2}{3D_f \lambda^2} \overline{R_g^2}\right)^{-D_f/2} \quad (2a-b)$$

where n^1 and n^2 are the first and second moments of the agglomerate size probability distribution function, R_g is the radius of gyration of the soot agglomerates, x_p is the optical size parameter ($x_p = \pi d_p / \lambda$), D_f is the fractal dimension, m is the complex index of refraction for soot, d_p is the soot primary particle

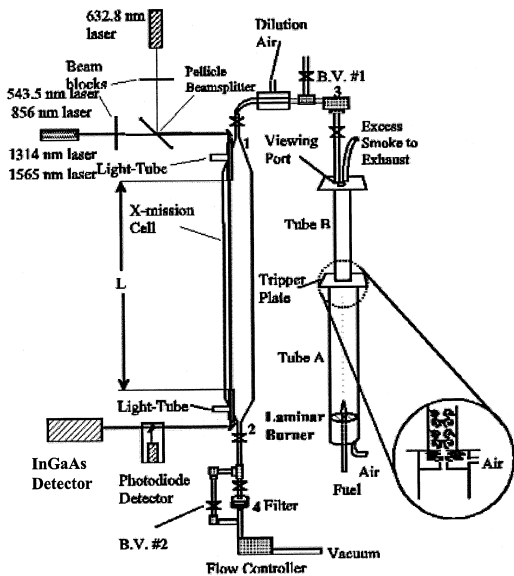


FIG. 1. Schematic of the LAOF with laminar diffusion flame burner.

diameter, and $E(m)$ and $F(m)$ are the functions of complex refractive index.

With the assumption that the interaction of soot particles with the incident radiation is in the Rayleigh scattering regime (for which scattering is negligible with respect to absorption), K_e (which is equal to K_a in the Rayleigh limit) can be calculated using the following equation with the reported refractive index of soot [6–9]:

$$K_e = \frac{36\pi n_s k_\lambda}{(n_\lambda^2 - k_\lambda^2 + 2)^2 + 4n_\lambda^2 k_\lambda^2} \quad (3)$$

There are, however, valid concerns regarding the accuracy of using this method for computing soot optical properties. Recent experiments [10–14] in the visible and near-IR spectrum indicate that the measured K_e values are significantly larger than the calculated value using equation 3 with $m = 1.57 - 0.56i$, which appears to be the most widely used value for the refractive index for soot [6,15].

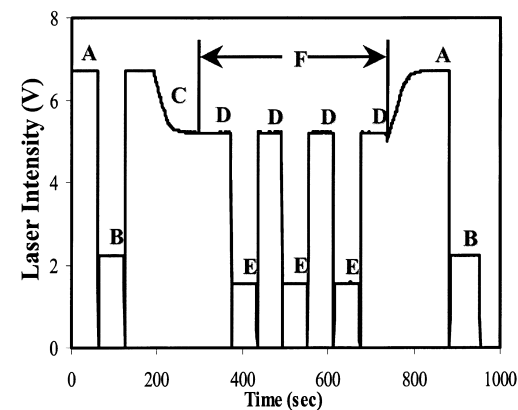
Recently, Zhu et al. [14] performed K_e measurements for laminar ethene and acetylene diffusion flame soot using an 856 nm laser light source. These experiments have illustrated some characteristics of the fuel and spectral dependence of K_e . The motivation for this investigation is to extend the measurements of K_e into the IR spectrum (up to 1565 nm) using the Large Agglomerate Optics Facility (LAOF) for soot produced in laminar diffusion flames. There are several important reasons for extending the measurements of K_e further into the IR. Larger soot concentrations (f_v) over longer path lengths (L) can be analyzed as a result of the lower

level of attenuation (due to the “ $1/\lambda$ ” term in the exponent of equation 1). Soot optical properties in the IR spectrum are also required for accurate two-wavelength pyrometry (for soot temperature measurements [16,17]) and for characterizing radiation heat transport in flames and fires [18–20]. In this study, measurements of K_e for acetylene and ethene soot performed at a variety of wavelengths are presented. These values of K_e will provide combustion researchers with reliable properties for accurate application of fuel- and wavelength-specific light extinction (for soot concentration) and two-wavelength pyrometry (for soot temperature) techniques.

Experimental Description of K_e Measurements

Experiments were performed using the National Institute of Standards and Technology LAOF to accurately measure optical properties of soot produced using laminar acetylene and ethene diffusion flames. A detailed description of the apparatus can be found in Mulholland and Choi [11]. Fig. 1 displays a schematic of the experimental apparatus, including the LAOF and laminar burner system. The laminar burner fuel nozzle has an i.d. of 11 mm, and the outer brass tube has an outer diameter of 108 mm. The smoke emitted by the flames is mixed with dilution air as it flows through a tripper plate. The mixture is further diluted with air prior to entrance into the transmission cell. A bypass valve (B.V. #1) is positioned directly before the diluter to purge the transmission cell with clean air before and after each experiment.

Light extinction measurements were performed using a 1 mW He-Ne laser operating at 543.5 nm, a 10 mW He-Ne laser operating at 632.8 nm, a 30 mW diode laser operating at 856 nm, a 3 mW diode laser operating at 1314 nm, and a 1.5 mW diode laser operating at 1565 nm. Measurements were performed using a combination of the 632.8 nm He-Ne laser (as a baseline for comparison and to eliminate the experiment to experiment uncertainty) and one of the other lasers (i.e., 543.5/632.8 nm, 856/632.8 nm, 1314/632.8 nm, and 1565/632.8 nm). A pellicle beam splitter was used (Fig. 1) to produce colinear beams through the transmission cell. The beams were directed through the cell to the detectors (a separate silicon photodiode and InGaAs photodiode detectors) using gold-coated mirrors and wedge optics. For the 543.5/632.8 nm and the 856/632.8 nm experiments, only the silicon photodiode detector was used. For experiments involving the 1314/632.8 nm and the 1565/632.8 nm combinations, both the silicon and the InGaAs photodiode detectors were used. An IR pass filter was placed in front of the InGaAs detector to discriminate against



A: Background monitoring of 856nm B: Background monitoring of 632.8 nm
 C: Soot into transmission cell D: Attenuation of 856 nm laser by soot.
 E: Attenuation of 632.8 nm laser by soot F: Soot collection period.

FIG. 2. Laser transmittance for soot extinction constant measurement (laser wavelengths of 632.8 and 856 nm combination).

the 632.8 nm light. Rotating beam blocks were attached in front of the light sources to selectively monitor the wavelength of interest.

For explanation of the general procedure used in all of the light-source combinations, the procedure for the 856/632.8 nm combination is described. After a steadily burning flame was established, the incident intensity of the transmitted beam at 856 nm was monitored for approximately 60 s (by blocking the beam at 632.8 nm, denoted by A in Fig. 2). The incident transmitted intensity at 632.8 nm was then measured for 60 s (by blocking the 856 nm beam, denoted by B). Soot was then introduced into the transmission cell. When the intensity ratio stabilized, the exhaust flow was directed through the filter to collect the soot (denoted by C). Simultaneously, the transmitted light intensity measurement was recorded. This procedure was repeated in alternating 60 s intervals for 856 nm (denoted by D) and 632.8 nm (denoted by E) wavelengths. The soot collection period was approximately 7 min, after which clean air was used to purge the cell (denoted by the end of F). The intensity measurements for both light sources were again performed to ascertain whether soot was deposited on the optical windows during the collection period. The mass of sampled soot, m_s , collected on glass fiber filter was then weighed using a microbalance (2–3 μg sensitivity). The K_e value was determined for each experiment using the following relationship:

$$K_e = \frac{-\ln\left(\frac{I}{I_0}\right)\lambda}{f_{vg}L} = \frac{-\ln\left(\frac{I}{I_0}\right)\lambda\rho_s}{m_sL} V \quad (4)$$

with the measured intensity ratio, I/I_0 , the volume

of the sampled gas, V , and the measured mass of the collected soot, m_s . Absolute calibration of the experiments was performed using an aerosol of monodisperse polystyrene spheres. The comparison of the measured K_e for the calibration aerosol to the actual value (using the known refractive index of the polystyrene spheres) indicates an error of less than 4%.

Experimental Description of Soot Sampling and Analysis

There have been numerous investigations for determining soot agglomerate structure using transmission electron microscopy (TEM) [21–25]. These studies have all demonstrated that soot agglomerate structures display universal characteristics despite the differences in the type of fuels burned and the flame configurations. Soot agglomerates are known to be composed of individual spherical primary particles that are connected to one another in point contact. Soot agglomerates have very broad size distributions that are functions of residence time. In many instances, the magnitude of the standard deviation of the agglomerate dimensions is as large as the mean value [24].

One of the limitations of using TEM analysis exclusively for soot structure analysis is that measurements can be biased toward the smaller agglomerates since the high magnification of TEM analysis precludes complete imaging of large agglomerates. Therefore, in this study, the TEM analysis was combined with optical microscope analysis to enable the analysis of broader agglomerate size distribution. The high magnification of the TEM allows for accurate measurements of R_g and d_p that are necessary for the calculation of fractal dimensions. The low magnification afforded by optical microscopes will result in a larger field of view to obtain a statistically meaningful number of the infrequently encountered (but important) large agglomerates with lengths greater than 3 μm .

Smoke samples were collected on TEM grids and microscope coverslips attached to a thermal precipitator. The sampler was located at the midsection of the transmission cell. The sampling time was selected to ensure that the coverage of soot sample on the TEM grid or microscope coverslips was less than 20%. The TEM grids and coverslips were analyzed using a JEOL 100-CX transmission electron microscope (at 13,000–26,000 magnification) and a Renishaw RamanScope 2000 optical microscope (at 1000–2000 magnification), respectively. Soot agglomerates on the TEM micrographs and microscope coverslips were digitized using a high-resolution CCD camera equipped with an 18–108 mm zoom lens.

Using the TEM images, the primary particle diameter, d_p , was measured with customized software

developed in the author's laboratory [26]. For each condition, more than 200 particles were measured to determine the average d_p . The average values of the d_p measurements are shown in Table 1. The projected area of the agglomerate, A_a , and the average area of the primary particle, A_p (determined by using the measurement of d_p) are used to determine the total number of primary particles that constitute each agglomerate, N , using the following relationship [27]:

$$N = \left(\frac{A_a}{A_p} \right)^{1.09} \quad (5)$$

The radius of gyration is measured by employing the following equation:

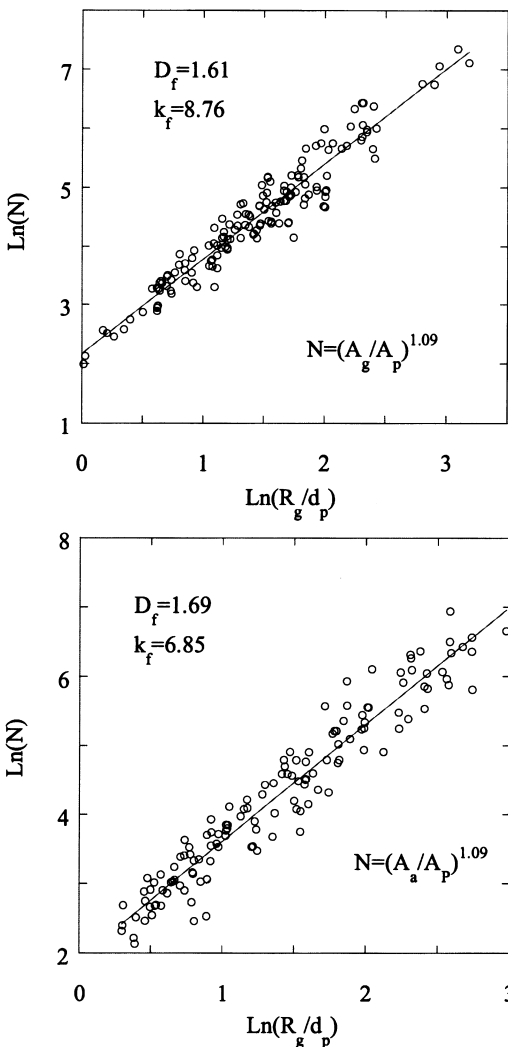


FIG. 3. Plot of $\ln(N)$ versus $\ln(R_g/d_p)$ for ethene and acetylene soot.

$$R_g = \sqrt{\frac{1}{N} \sum_{i=1}^N r_i^2} \quad (6)$$

where r_i is the distance between the center of an individual primary particle and the agglomerate centroid. Since it is difficult to identify each particle within the agglomerate, the R_g calculation formulation in equation 6 was revised by considering each pixel constituting the agglomerate as the element of interest. The value of N in equation 6 was replaced by n , which is the total number of pixels constituting the soot agglomerate. This substitution is valid since the average contribution to the total R_g from the subelements (pixels) that constitute the primary particle is equal to the contribution from a primary particle to the total R_g . Fig. 3 displays the plot of $\ln(N)$ versus $\ln(R_g/d_p)$ for ethene and acetylene soot for which the slope represents D_f and the intercept represents $\ln(k_f)$. Table 1 displays the measured soot agglomerate structure properties of D_f and k_f .

The mean value of R_g measured using the TEM analysis is not the representative mean value since high magnifications used in the TEM analysis preclude detection of large agglomerates. The representative mean value of the R_g (geometric mean R_g calculated based on soot agglomerate size distribution [26]) was measured using the combined TEM and optical microscopy method. In this method, size classes of agglomerates were divided with equal spacing in terms of the logarithm of agglomerate size, as is widely done for broad aerosol size distributions [28]. For example, all of the agglomerates in the size class between 1 and 2 μm are in one class, those agglomerates between 2 and 4 μm are in another class, and so on. In the optical microscope analysis, the agglomerates were sized in terms of $(LW)^{1/2}$, where L and W are the length and width (perpendicular to the direction in which L was measured) of the agglomerate, respectively. More than 1500 agglomerates were analyzed for both the TEM and optical microscopy. The optical microscope data was scaled so that the TEM and optical microscope results were in correspondence for agglomerates in the size class with $(LW)^{1/2}$ between 1 and 2 μm . The size distribution is expressed in terms of R_g by dividing the geometric mean of the $(LW)^{1/2}$ for each size class by the factor 2.56 [26]. Measurements indicate

TABLE 1
Morphology measurement of soot produced from laminar flamelets

	d_p (nm)	k_f	D_f	N	R_g (nm)
Ethene	36.7 ± 10.1	6.85	1.69	162	175
Acetylene	50.9 ± 4.7	8.76	1.61	149	241

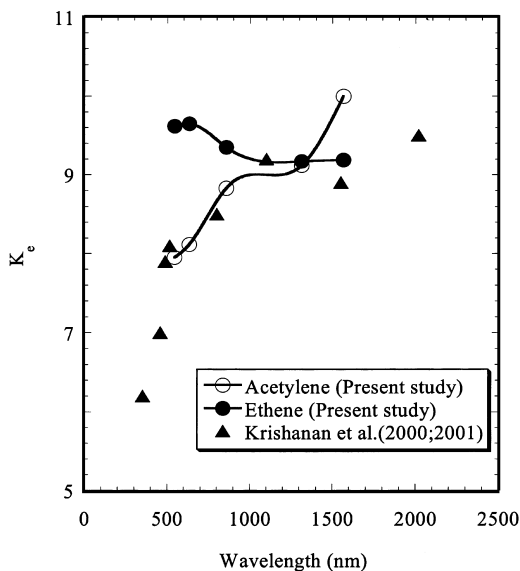


FIG. 4. Measured dimensionless extinction constant K_e for soot produced from acetylene and ethene laminar diffusion flames in the wavelength range from 543.5 to 1565 nm.

that the geometric mean of R_g ranges from 18 to 8.84 μm . The acetylene distribution is shifted to a slightly larger size with a geometric mean for R_g of 241 nm versus 175 nm for the ethene (Table 1).

Discussions

Figure 4 and Table 2 display the measured K_e and the uncertainty (95% confidence level) for acetylene and ethene soot from laminar diffusion flame light source wavelengths ranging from 543.5 to 1565 nm. The uncertainty limits correspond to the estimated total expanded uncertainty (95% confidence level) based on type B and type A uncertainties [29]. The type B uncertainties are based on scientific judg-

ment rather than statistical means and equal 2.7% of the mean value [11]. The type A uncertainties (which are evaluated by statistical methods) are based on typically five repeat measurements on each of three days equal about 0.5% of the mean for ethene and about 2% of the mean for acetylene. Measurements of K_e in the IR spectrum for soot emitted from large buoyant turbulent diffusion flames by Krishnan et al. [13,30] are also shown in Fig. 4. It is seen that their results agree within about 10% with the acetylene results over the wavelength range from about 543 to 1565 nm. Their results are reported as average values for the various gaseous and liquid fuels. For acetylene soot, the K_e increases from a value of 7.95 at 543.5 nm to 10.0 at 1565 nm. The ethene K_e , on the other hand, was relatively constant, with K_e varying from 9.62 at 543.5 nm to 9.19 at 1565 nm. The utility of the new IR measurements is best demonstrated in its application for conditions involving long pathlengths and/or higher soot concentrations that would be rendered optically thick in the visible spectrum. For example, at $\lambda_2 = 1565$ nm compared to $\lambda_1 = 543.5$ nm, the product of (fL) that can be analyzed is increased by a factor of

$$\frac{\lambda_2}{\lambda_1} \frac{K_{e1}}{K_{e2}} = 2.28$$

where K_{e2} and K_{e1} are the values of extinction constant for acetylene at the two wavelengths. Another benefit of performing light extinction measurements in the near IR results is that the difference in the values of the K_e for the two fuels is also reduced with increasing wavelength. At 543.5 nm, the difference is 19% with respect to the mean value. For 1565 nm, on the other hand, the difference in K_e is reduced to 9% with respect to the mean value, thereby reducing the uncertainty in measurements when a universal value of K_e is established for use in light extinction measurements.

The variation of K_e for acetylene soot with wavelength may be caused by beam-shielding effects. Beam shielding is caused by the attenuation of light incident upon particles on the leeward side of the

TABLE 2
Summary of measured and predicted dimensionless extinction constant K_e from the literature

λ (nm)	Meas. K_e Acetylene	Meas. K_e Ethene	Pred. K_e Ref. [6]	Pred. K_e Ref. [7]	Pred. K_e Ref. [8]	Pred. K_e Ref. [9]
543.5	7.95 ± 0.44	9.62 ± 0.46	4.90	4.84	2.94	4.51
632.8	8.12 ± 0.44	9.65 ± 0.40	4.87	4.55	2.69	4.29
856	8.83 ± 0.52	9.35 ± 0.38	5.20	3.81	2.55	4.11
1314	9.12 ± 0.62	9.17 ± 0.46	5.92	2.68	2.93	4.31
1565	10.0 ± 0.80	9.19 ± 0.48	6.10	2.28	3.24	4.51

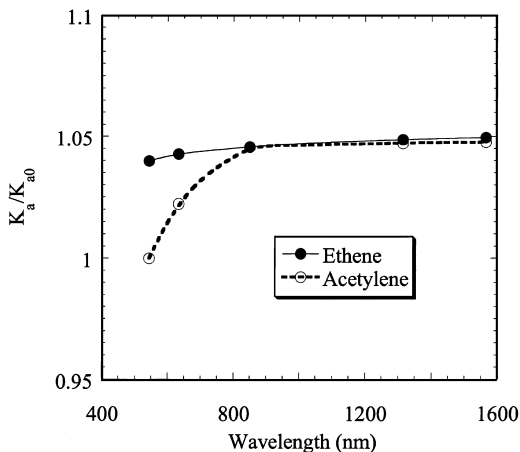


FIG. 5. Normalized soot absorption constants calculated using predictions of beam-shielding effects [31] for both acetylene and ethene.

agglomerates due to blockage by particles on the forward side. If beam-shielding effects were not present, absorption by an agglomerate may be considered to be the product of the absorption by a single particle (representative of the average within the agglomerate) and the total number of particles constituting the agglomerate. The magnitude of absorption decreases with the degree of beam shielding by overlapping particles in the direction of laser-beam propagation. Thus, with each successive passage through the intervening particles (with attendant reduction in intensity), the particles on the leeward side experience a smaller magnitude of incident intensity and a smaller amount of absorption. The larger soot particle dimensions can lead to acetylene soot being more susceptible to beam-shielding effects compared to ethene.

Numerical modeling of the beam-shielding effect (screening effect in Mulholland and Mountain [31]) demonstrates that this phenomenon can cause a measurable reduction of the soot extinction constant. Mulholland and Mountain [31] computed the mass specific extinction coefficient (which is proportional to dimensionless extinction constant K_e) for computer-generated soot clusters with 3–1390 primary spheres using a coupled electric and magnetic dipole (CEMD) method. Computed mass specific absorption constants, σ_a (which are proportional to K_{a0} , dimensionless absorption constant), were plotted as function of the number of primary spheres that constitute agglomerates for different optical size parameters, x_p [31]. Their results indicate that for the same agglomerate structure (i.e., fractal dimension and prefactor), the effect of beam shielding increases with optical size parameter, x_p , and the number of particles that constitute the agglomerate. Soot morphology measurements produced an average d_p

of 36.7 nm for ethene soot and 50.9 nm for acetylene soot. The corresponding changes in x_p were from 0.21 to 0.07 for ethene and from 0.29 to 0.10 for acetylene as the wavelength is varied from 543 to 1565 nm. The average number of primary particles constituting aggregates was calculated to be 149 for acetylene and 162 for ethene (the linear average of N values for acetylene and ethene were calculated using the number size distribution [26]). Using the results of Mulholland and Mountain [31], the normalized soot absorption constants are plotted as a function of wavelength for ethene and acetylene soot in Fig. 5. The acetylene K_a increases slightly with wavelength in the visible spectrum and levels off in the near-IR spectrum as the size parameter decreases. The prefactor term, k_f , is another important factor that may influence beam shielding. Results from soot morphology analysis indicate acetylene soot agglomerates have a k_f value of 8.76 versus 6.85 for ethene soot. The physical interpretation of k_f relates to the compactness or the level of packing of the soot particles for a given agglomerate with the same projected area. A higher value of k_f for acetylene flame soot translates into more overlapping of soot particles in the direction of incident light.

For ethene soot, the magnitude of the reduction in K_e due to the beam-shielding effect is expected to be smaller than for acetylene soot cases because of the smaller d_p and less compact agglomerate structure. Furthermore, the slight reduction in K_e with wavelength observed for ethene is contrary to the trend expected for beam shielding. This behavior is more likely attributed to the reduction of the scattering constant, K_s . Under this scenario, because of the smaller d_p , smaller number of primary particles constituting the agglomerate, and less compact agglomerate structure, the ethene K_a will essentially remain constant (as predicted by the CEMD theory).

In a previous study, Zhu et al. [26] performed measurements of the K_s constant for soot produced in laminar ethene and acetylene flames at wavelengths of 543.5, 632.8, and 856 nm. Combining the scattering measurements from Zhu et al. [26] with extinction measurements in the present study, the spectral dependence of K_a ($K_a = K_e - K_s$) was determined. Fig. 6 displays the measured K_a for acetylene and ethene soot. The measurements indicate that the acetylene K_a increases with wavelength (as predicted by the CEMD model [31]), varying from 5.44 to 6.72 from 543.5 to 856 nm. The level of increase in the measured K_a (~24%) for acetylene, however, is much larger than the value (~5%) predicted using the CEMD theory with the assumption of a constant refractive index. The reason for this large difference is not known. The ethene K_a , however, remains nearly constant, varying only from 7.25 to 7.51 for the same wavelength range, in correspondence with the prediction of the CEMD theory.

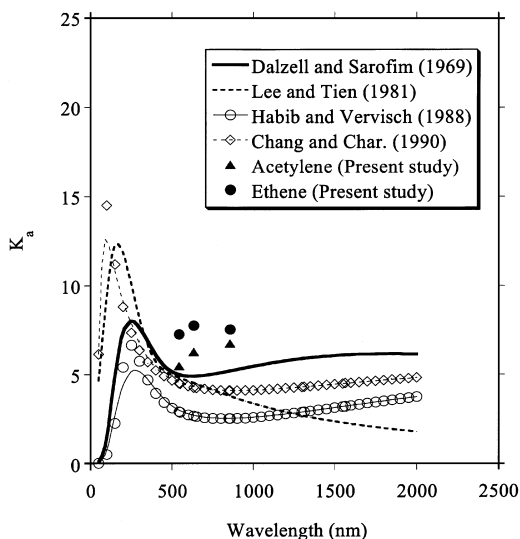


FIG. 6. Measured and calculated soot dimensionless absorption constant, K_a , for acetylene and ethene produced from laminar diffusion flames.

It is of importance to compare our measurements of K_a to K_a values predicted using equation 3 together with results derived from refractive index measurements [6–9]. The reader may recall that the K_a is essentially equal to K_e under conditions of negligible scattering. The reported refractive index values from the various sources were obtained using different experimental techniques and theoretical treatments of the interaction of soot with light. For example, Dalzell and Sarofim [6] used compacted soot pellets from propane and acetylene flames and performed *ex situ* reflectance/transmission measurements at room temperature between 0.4358 and 0.8065 μm and from 2.5 to 10 μm . Using the measurements for propane soot, they applied the Drude-Lorentz dispersion relationship based on the optical transitions of bound and free electrons to predict the variations in the refractive index in the near-IR range. In 1981, Lee and Tien [7] analyzed light extinction measurements of polystyrene and Plexiglas flames to develop a dispersion relationship (for a range encompassing 0.3 to 20 μm) in which the damping constants of the free and bound electrons were determined rigorously with experimental validation rather than estimations based on graphite results [6]. In 1988, Habib and Vervisch [8] performed *in situ* transmission measurements for premixed flames of methane, propane, and ethylene from 0.4 to 4.5 μm , from which a dispersion relationship following the method of Lee and Tien [7] was employed. In 1990, Chang and Charalampopoulos [9] performed *in situ* dynamic light scattering and extinction measurements in premixed propane flames

from 0.2 to 6.4 μm . In their analysis, the spectral dependence of the refractive index was derived through the application of the Kramers-Krönig model. Fig. 6 also displays the calculated K_a values using the refractive indices derived from the Drude-Lorentz dispersion relationships [6–8] or the Kramers-Krönig relationships [9]. The large differences in the spectral variation of measured K_a with predicted K_a indicates that the practice of employing reported refractive indices may not be valid for analyzing soot concentration using light extinction techniques.

Conclusions

The spectral variations of K_e measured for soot from laminar acetylene and ethene flames range from 7.95 to 10.0 and from 9.17 to 9.65, respectively. These results represent the first measurements of fuel and wavelength-dependent K_e for soot produced from laminar diffusion flames. The present measurements have provided important information regarding the absorption and extinction properties of soot in the visible and near-IR spectrum. These measurements provide accurate data that can be used for more reliable soot concentration and temperature measurements using light extinction and two-wavelength pyrometry techniques.

The values of K_e for ethene remained nearly constant with increased wavelength, which indicates that any increase in the absorption coefficient with wavelength (due to beam shielding) is offset by a reduction in the scattering constant. The cause of the observed increase of K_e of acetylene with wavelength (as opposed to the near-constant values of K_e for ethene) is not known. The larger primary particle and agglomerate dimensions of acetylene compared to ethene can only account for a small fraction of the increase. Analysis indicates that errors in f_i measurements are as large as a factor of 3 if the traditional method of using the Rayleigh limit solution is employed. The convergence of K_e values for acetylene and ethene soot suggests that errors related to the use of a universal K_e value will be reduced in the near-IR spectrum.

Acknowledgments

JYZ and MYC would like to acknowledge financial support from the Sandia National Laboratories (BF 9592). The authors wish to acknowledge the able assistance in measurements provided by Mr. Marco Fernandez of NIST.

REFERENCES

1. Hiltz, J. P., "Studies Say Soot Kills up to 60,000 in U.S. Each Year," *New York Times*, July 19, 1993, p. A1.

2. Dickerson, R. R., Kondragunta, S., Stenchikov, G., Civerolo, K. L., Doddridge, B. G., and Holben, B. N., *Science* 278(5339):827 (1997).
3. McDow, S. R., Vartiainen, M., Sun, Q. R., Hong, Y. S., Yao, Y. L., and Kamens, R. M., *Atmos. Environ.* 29(7):791 (1995).
4. Ammann, M., Kalberer, M., Jost, D. T., Tobler, L., Rossler, E., Piguet, D., Gaggeler, H. W., and Baltensperger, U., *Nature* 395(6698):157 (1998).
5. Dobbins, R. A., Mulholland, G. W., and Bryner, N. P., *Atmos. Environ.* 28:889 (1994).
6. Dalzell, W. H., and Sarofim, A. F., *J. Heat Transfer* 91:100 (1969).
7. Lee, S. C., and Tien, C. L., *Proc. Combust. Inst.* 18:1159 (1980).
8. Habib, Z. G., and Vervisch, P., *Combust. Sci. Technol.* 59:261 (1988).
9. Chang, H., and Charalampopoulos, T. T., *Proc. R. Soc. London, Ser. A* 430:577 (1990).
10. Choi, M. Y., Mulholland, G. W., Hamins, A., and Kashiwagi, T., *Combust. Flame* 102:161 (1995).
11. Mulholland, G. W., and Choi, M. Y., *Proc. Combust. Inst.* 27:1515 (1998).
12. Zhou, Z. Q., Ahmed, T. U., and Choi, M. Y., *Exp. Thermal Fluid Sci.* 18(1):27 (1998).
13. Krishnan, S. S., Lin, K. C., and Faeth, G. M., *J. Heat Trans.* 122:517 (2000).
14. Zhu, J., Choi, M. Y., Mulholland, G. W., and Gritzko, L. A., *Int. J. Heat Mass Transfer* 43:3299 (2000).
15. Smyth, K. C., and Shaddix, C. R., *Combust. Flame* 107:314 (1996).
16. Klassen, M., and Gore, J. P., *Combust. Flame* 93:270 (1993).
17. Choi, M. Y., Hamins, A., Mulholland, G. W., and Kashiwagi, T., *Combust. Flame* 99:174 (1994).
18. Grosshandler, W. L., *RADCAL: A Narrow-Band Model for Radiation Calculations in a Combustion Environment*, NIST technical note 1402, National Institute of Standards and Technology, Gaithersburg, MD, 1992.
19. Ezekoye, O. A., and Zhang, Z., *Combust. Flame* 110:127 (1997).
20. Gritzko, L. A., Sivathanu, Y. R., and Gill, W., *Combust. Sci. Technol.* 139:113 (1998).
21. Dalzell, W. H., Williams, G. C., and Hittel, H. C., *Combust. Flame* 14:161 (1970).
22. Dobbins, R. A., and Megaridis, C. M., *Langmuir* 3:254 (1987).
23. Erikson, W. D., Williams, G. C., and Hittel, H. C., *Combust. Flame* 8:127 (1964).
24. Köyliü, Ü. Ö., and Faeth, G. M., *Combust. Flame* 89:140 (1992).
25. Samson, R. J., Mulholland, G. W., and Gentry, J. W., *Langmuir* 3:272 (1987).
26. Zhu, J., Choi, M. Y., Mulholland, G. W., and Gritzko, L. A., *Proc. Combust. Inst.* 28:439 (2000).
27. Megaridis, C. M., and Dobbins, R. A., *Combust. Sci. Technol.* 71:95 (1990).
28. Cadle, R. D., *The Measurement of Airborne Particles*, Wiley, New York, 1975.
29. Taylor, B. N., and Kuyatt, C. E., *Guidelines for Evaluating and Expressing Uncertainty of NIST Measurements Results*, NIST technical note 1297, National Institute of Standards and Technology, Gaithersburg, MD, 1994.
30. Krishnan, S. S., Lin, K. C., and Faeth, G. M., *J. Heat Transfer*, 123:331 (2001).
31. Mulholland, G. W., and Mountain, R. A., *Combust. Flame* 119:45 (1999).